Temperature and density fluctuations in the inner Orion Nebula

W. J. Henney, C. R. O'Dell, G. J. Ferland, M. Peimbert

1. Analysis

1.1. Deriving diagnostic line ratios from WFC3 filter images

Note: this is similar to what I wrote in the the calibration draft, but specifically tailored to line ratios rather than equivalent widths. We may in the end want to move some of it back to the other paper.

The WFC3 camera is equipped with filters that effectively target important nebular diagnostic lines. Each filter, with label j, is characterized by an effective transmission profile, or throughput, T_λ^j, which gives the wavelength-dependent conversion factor between the number of photons arriving at the *HST* entrance aperture (nominal radius: 120 cm) and the number of electrons registered by the CCD, accounting for occultation by the secondary mirror, all other optical and quantum efficiencies, and the amplifier gain. The peak value of the filter transmission profile is denoted $T_{\rm m}^j$, with typical values of 0.2–0.3, and the "rectangular width" of the profile is defined as

$$W_j = (T_{\rm m}^j)^{-1} \int_0^\infty T_\lambda^j \, d\lambda \qquad [W_j] = \text{Å}. \tag{1}$$

Extensive and continuing on-orbit calibration of the filters has been carried out (Kalirai et al. 2009, 2010; Sabbi & the WFC3 Team 2013) using white dwarf standard stars. However, since these are flat featureless continuum sources, the calibration is only sensitive to the integrated filter throughput, given by the product $W_j T_{\rm m}^j$. A general increase in the integrated throughput of 10–20% with respect to pre-launch measurements was found for all filters, which was fitted by a low-order polynomial as a function of frequency. Only the broad-band and medium-band filters were used in determining the fit, but the scatter of the narrow-band filters[1] around the resulting curve is only a few percent (see Fig. 6 of Kalirai et al. 2009).

Emission lines from photoionized regions are intrinsically much narrower than even the narrowest WFC3 filters, so the transmission of such a line, with label i, is independent of W_j and depends instead solely on the throughput at the line wavelength: $T_i^j \equiv T_\lambda^j(\lambda = \lambda_i)$. The detailed shape of the throughput curves was measured pre-launch (Brown 2006), but direct on-orbit confirmation of these curves is impossible. However, by comparing WFC3 images with ground-based spectrophotometry of emission line nebulae, it is possible to test the filter calibrations for the case where emission lines are the dominant component of the spectrum in the filter bandpass. Just such a calibration is described in detail in a companion paper (Henney et al. 2014), using multiple spectrophotometric datasets of the Orion Nebula (M42) and the evolved nearby planetary nebula NGC 6720 (the Ring Nebula), and building on an earlier study in O'Dell et al. (2013). The conclusion of this study is that the nominal filter parameters (that is, the pre-launch measurements of the shape of the throughput curve T_λ^j, combined with the on-orbit re-calibration of $W_j T_{\rm m}^j$), are consistent to within ±5% with the emission line spectrophotometry for all but a handful of filters. The largest discrepancy is found for the F469N filter, which is found to have a sensitivity to the He II λ4696 line that is 35% higher than the nominal

[1] Note, however, that the quad filters were not included in these studies.

value. However, that line is absent in M42, due to the relatively low effective temperature of the ionizing star, and the filter is instead dominated by continuum and weak [Fe III] lines. In such circumstance the nominal F469N parameters are found to be accurate.

Smaller, but still significant, discrepancies are found for the F658N and FQ575N filters, which target the [N II] lines λ6583 and λ5755, respectively.

For the strongest lines, such as [N II]6583 In order to accurately calculate emission line ratios from WFC3 images, it is important to properly account for the contamination

1.2. Deriving T_e, n_e from line ratios

1.3. Analysis of fluctuations in T_e, n_e

REFERENCES

Brown, T. M. 2006, Filter Throughputs for WFC3 SYNPHOT Support, Instrument Science Report WFC3 2006-3, Space Telescope Science Institute, Baltimore

Henney, W. J., O'Dell, C. R., Ferland, G. J., & Peimbert, M. 2014, In prep

Kalirai, J. S., Baggett, S., Borders, T., & Rajan, A. 2010, The Photometric Performance of WFC3/UVIS: Temporal Stability Through Year 1, Instrument Science Report WFC3 2010-14, Space Telescope Science Institute, Baltimore

Kalirai, J. S., et al. 2009, WFC3 SMOV Proposal 11450: The Photometric Performance and Calibration of WFC3/UVIS, Instrument Science Report WFC3 2009-31, Space Telescope Science Institute, Baltimore

O'Dell, C. R., Ferland, G. J., Henney, W. J., & Peimbert, M. 2013, AJ, 145, 92

Sabbi, E., & the WFC3 Team. 2013, WFC3 Cycle 20 Calibration Program, Instrument Science Report WFC3 2013-05, Space Telescope Science Institute, Baltimore

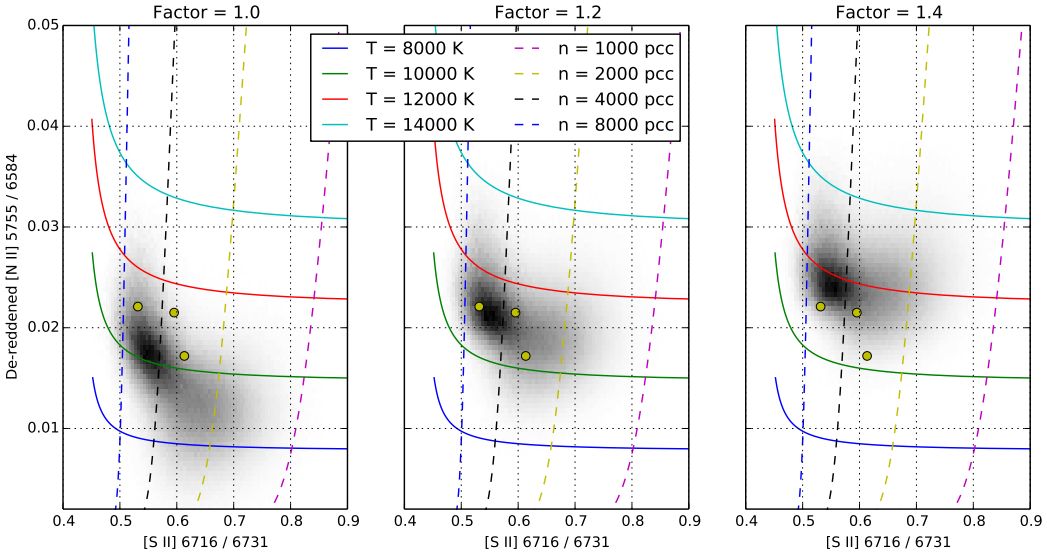

Fig. 1.— Distribution of line ratios

(*a*) (*b*)

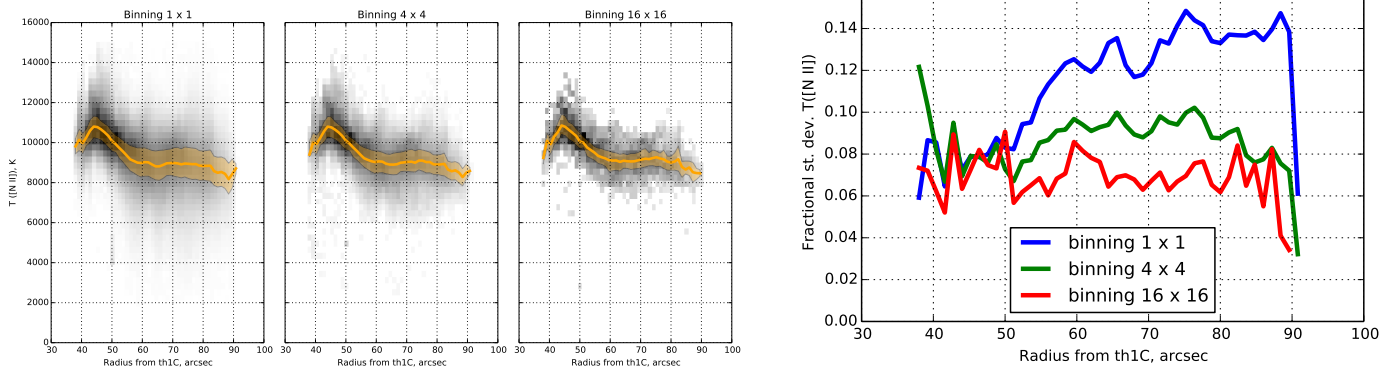

Fig. 2.— (*a*) Temperature distribution as a function of radius for different binnings. (*b*) Standard deviation of temperatures as a function of radius for different binnings.

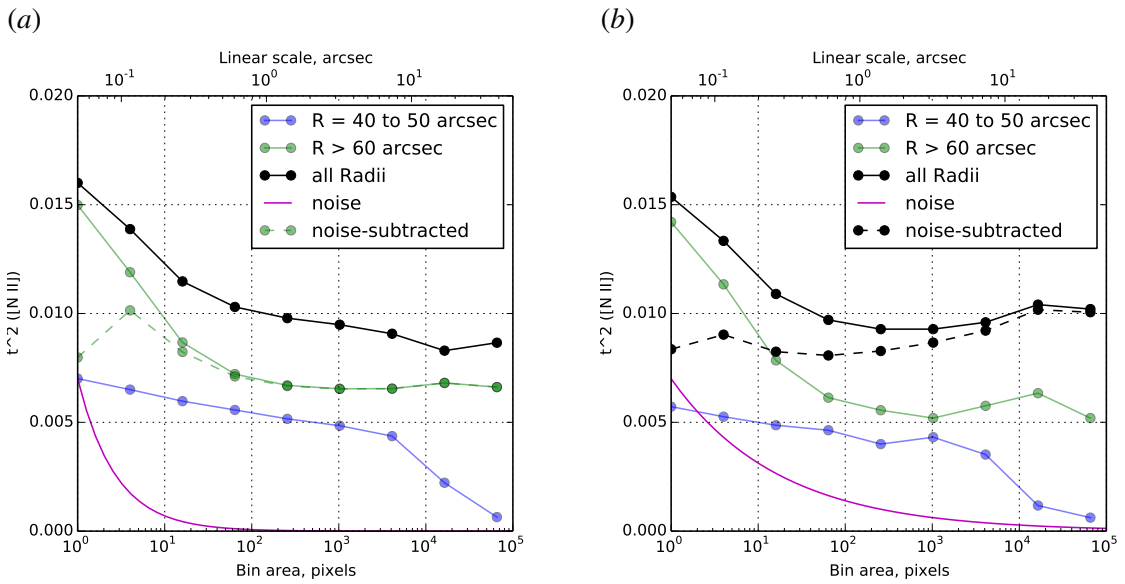

Fig. 3.— Scale-dependence of temperature fluctuations: t^2 as a function of binning. (*a*) Variance of $T_e/\bar{T}_e$ for the entire image (black line) and two subsamples: an annulus centered on the high-temperature region (blue line) and the more distant, fainter regions (green line). The magenta line is an estimate of the noise contribution to the full sample, and the dashed black line is the result of subtracting the noise from the observed values. (*b*) Same as *a* but using a "robust" estimator of the variance, based on the interquartile range.

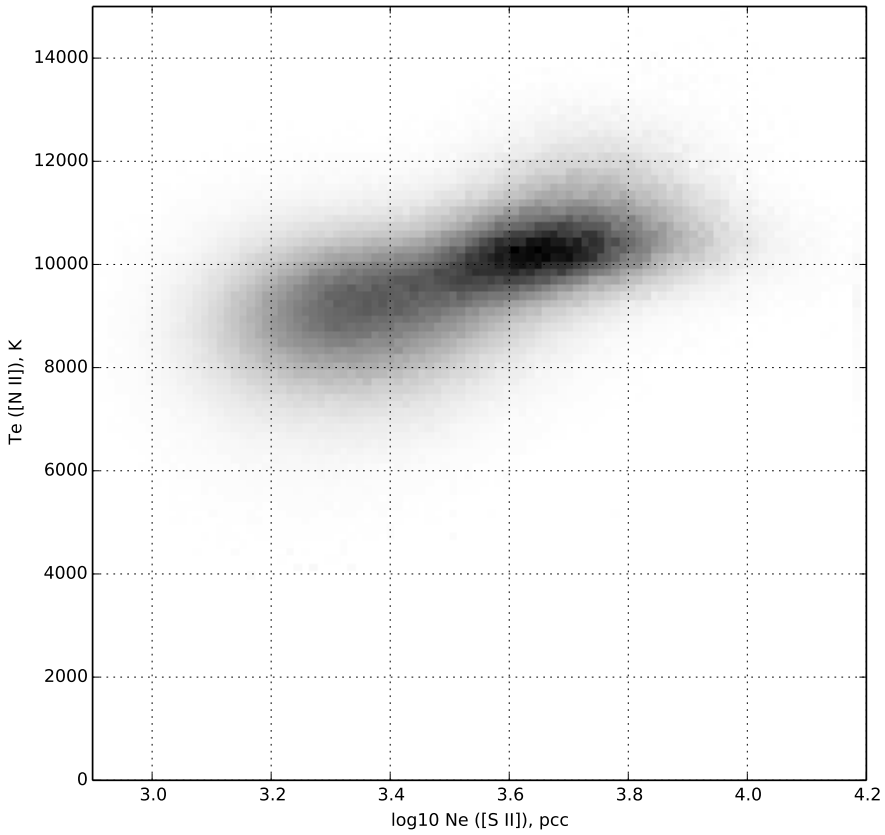

Fig. 4.— Joint distribution of temperature and electron density for low ionization regions.

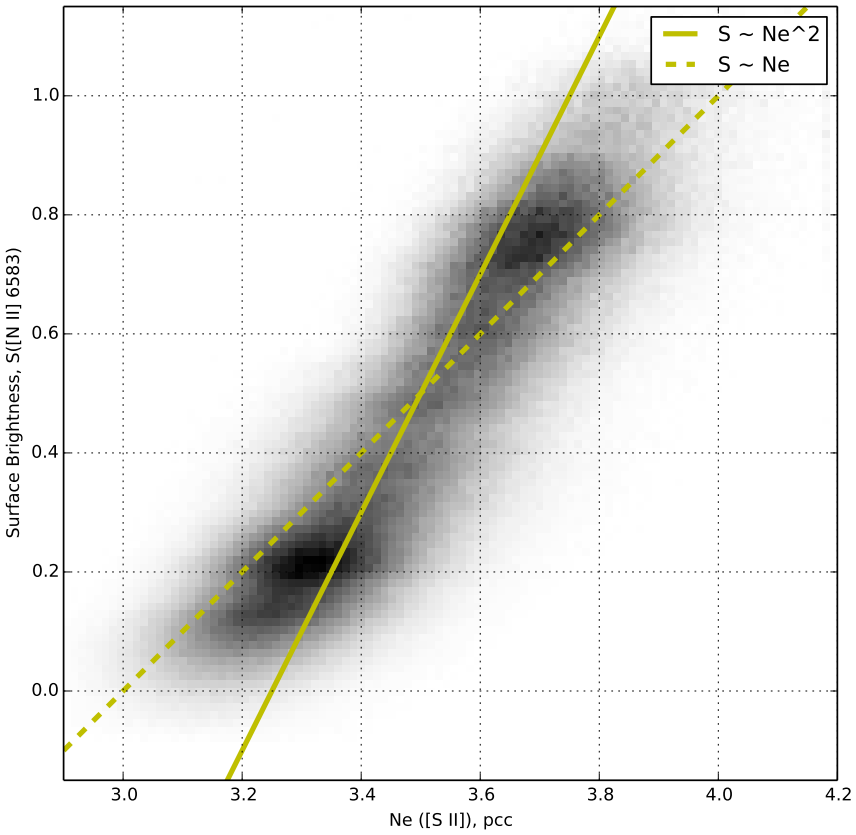

Fig. 5.— Correlation between [S II] density and [N II] surface brightness.